

# InternVL-X: Advancing and Accelerating InternVL Series with Efficient Visual Token Compression

Dongchen Lu<sup>1</sup>    Yuyao Sun<sup>2</sup>    Zilu Zhang<sup>1</sup>    Leping Huang<sup>1</sup>  
 Jianliang Zeng<sup>3</sup>    Mao Shu<sup>1\*</sup>    Huo Cao<sup>1\*</sup>

<sup>1</sup> Baidu Inc.

<sup>2</sup> Xidian University

<sup>3</sup> University of Chinese Academy of Sciences

\* Corresponding Author

## Abstract

Most multimodal large language models (MLLMs) treat visual tokens as “a sequence of text”, integrating them with text tokens into a large language model (LLM). However, a great quantity of visual tokens significantly increases the demand for computational resources and time. In this paper, we propose InternVL-X, which outperforms the InternVL model in both performance and efficiency by incorporating three visual token compression methods. First, we propose a novel vision-language projector, PVTC. This component integrates adjacent visual embeddings to form a local query and utilizes the transformed CLS token as a global query, then performs point-to-region cross-attention through these local and global queries to more effectively convert visual features. Second, we present a layer-wise visual token compression module, LVTC, which compresses tokens in the LLM’s shallow layers and then expands them through upsampling and residual connections in the deeper layers. This significantly enhances the model’s computational efficiency. Furthermore, we propose an efficient high resolution slicing method, RVTC, which dynamically adjusts the number of visual tokens based on image area or length filtering. RVTC greatly enhances training efficiency with only a slight reduction in performance. By utilizing 20% or fewer visual tokens, InternVL-X achieves state-of-the-art performance on 7 public MLLM benchmarks, and improves the average metric by 2.34% across 12 tasks. The source code is available at <https://github.com/ludc506/InternVL-X>.

## 1. Introduction

MLLMs, such as BLIP [11, 24, 25], LLaVA [23, 32–34], QwenVL [2, 47], InternVL [7, 8] have demonstrated remarkable progress in recent years, showcasing impressive

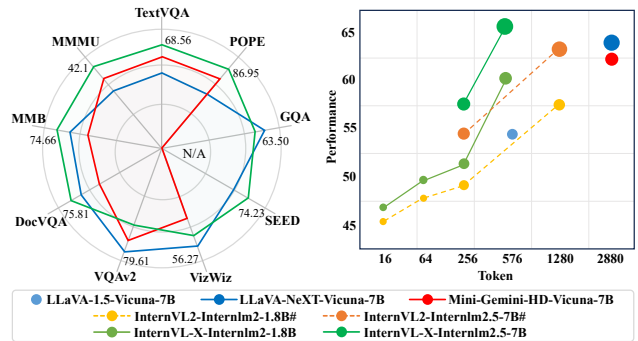


Figure 1. Comparison between InternVL-X and other models. # indicates the model is not an official checkpoint, but a version we retrained.

performance across various vision-language tasks such as visual question answering, image captioning, etc. MLLMs are attracting more attention from the academia and open-source community.

Currently, most MLLMs adopt the LLaVA framework, where images are initially processed by a visual encoder to extract visual embeddings. These embeddings are then converted through a vision-language projector to make them interpretable by LLMs. Subsequently, LLMs process the joint representation of visual and text embeddings. Typically, LLMs have parameter capacities that exceed those of Vision Transformers (ViT) [14] by several orders of magnitude, thereby dominating the computational requirements in multimodal architectures. Additionally, the number of visual tokens can range from hundreds to thousands, contributing to significant processing delays even for simple tasks. Consequently, visual token compression has become an area of increasing interest for researchers.

Previous visual token compression approaches for multimodal models typically focus on optimizing individual components in isolation. BLIP2 and QwenVL employ

learnable queries and cross-attention to extract key information from the full set of visual tokens. InternVL applies pixel-shuffle to merge adjacent tokens within a grid. FastV [6] utilizes text-guided attention during the LLM stage to selectively retain important visual tokens. However, these optimization strategies fail to fully exploit the potential for model acceleration, as they overlook the opportunities of joint optimization across different components.

To address this limitation, we propose InternVL-X, which builds upon the InternVL series by incorporating three complementary visual token compression methods: Projector Visual Token Compressor (PVTVC), Layer-wise Visual Token Compressor (LVTC), and Resolution Visual Token Compressor (RVTC). Each of these modules can independently accelerate the model while also complementing one another.

PVTVC begins by dividing visual embedding into non-overlapping grids based on its 2D space. It employs a point-to-region cross-attention that utilizes two distinct queries to extract features from the grid effectively. The local query is generated by downsampling the visual tokens within the grid, while the global query is derived from the CLS token. This combination of queries allows the model to maintain a balanced integration of detailed local information and comprehensive global semantics.

By visualizing the attention of InternVL, we observe that most visual tokens receive low attention in the early stage of LLM, and the attention distance gradually expands as the model deepens. LVTC compresses tokens at the input layer and restores them at deep layers. To mitigate information loss during this process, we introduce multiple visual information injection paths through learnable projectors and residual connections. LVTC significantly improves the computational efficiency at different LLM stages.

Current high resolution methods, like InternVL’s ratio slicing strategy, often result in computational inefficiencies when processing images with low pixel counts but extreme aspect ratios. RVTC uses the original image’s pixel count or edge length to determine the optimal number of slices, effectively reducing visual token numbers. While maintaining a minimal decrease in performance, RVTC significantly enhances training efficiency.

Our main contributions can be summarized as follows:

- 1) We propose three token compression modules that effectively reduce the number of visual tokens across different MLLM stages, which significantly accelerates MLLM.

- 2) Through extensive experiments, we demonstrate that each module can independently improve computational efficiency. Moreover, combining these modules not only significantly accelerates training speed but also maintains or even enhances model performance.

- 3) Leveraging these modules, we present the InternVL-X model series and compare it with other MLLMs across a

wide range of multimodal tasks. Our model achieves state-of-the-art results, outperforming other open-source models by a significant margin across multiple benchmarks.

## 2. Related Work

### 2.1. MLLM

In recent years, the field of MLLMs has rapidly evolved. Most MLLMs integrate LLMs with advanced visual encoders through a simple projector. BLIP series [11, 25], MiniGPT4 [56], and QwenVL [2] utilize Q-Former (cross-attention) to effectively align vision-text features and extract visual information. Flamingo [1] adopts gated cross-attention to deliver encoded image information into the layers of LLMs. LLaVA series [23, 32–34] proposes a two-layer MLP structure to bridge vision and language models. Several subsequent works, like VILA [30], ShareGPT4V [5], DeepSeekVL [37], CogVLM [48], InternVL [7, 8], etc. have followed this architecture.

### 2.2. Visual token compression

Existing visual token compression methods can be broadly classified into two categories: compression during the visual projection stage, and LLM stage.

Extensive research has focused on token compression at the projection stage. Resample [2] and Q-former [25] use learnable queries to compress token number and extract visual features through cross-attention. Abstractor [4] and LDP [9, 10] adopt multi-layer convolution structures to enable local token interactions while preserving spatial relationships. Pixel-shuffle [8] efficiently compresses tokens by transforming spatial dimensions into feature dimensions while preserving spatial context. TokenPacker [26] downsamples visual tokens to generate queries, then employs point-to-region attention to extract information from original tokens, preserving fine-grained details in the compressed tokens. FasterVLM [52] and LLaVA-PruMerge [42] selectively retain visual tokens based on their attention scores with the CLS token. LLaVA-Prumerge employs clustering techniques to merge discarded tokens, aiming to minimize information loss. TRIM [45] leverages the CLIP [41] metric to evaluate the significance of each visual token. LLaVA-Mini [53] incorporates a pre-fusion module to inject visual information into text tokens to mitigate performance degradation caused by compression.

Alternatively, several methods implement compression at the LLM stage. FastV [6] computes the attention between vision and text tokens from the 2-nd layer of LLM and retains the top-k tokens with the highest attention scores. FiCoco [18] improves upon FastV by merging similar discarded tokens to minimize visual information loss. SparseVLM [54] evaluates the visual token importance through a vision-text matrix and proposes a rank-based strategy to adaptively determine the compression ratio. MustDrop [35] pro-

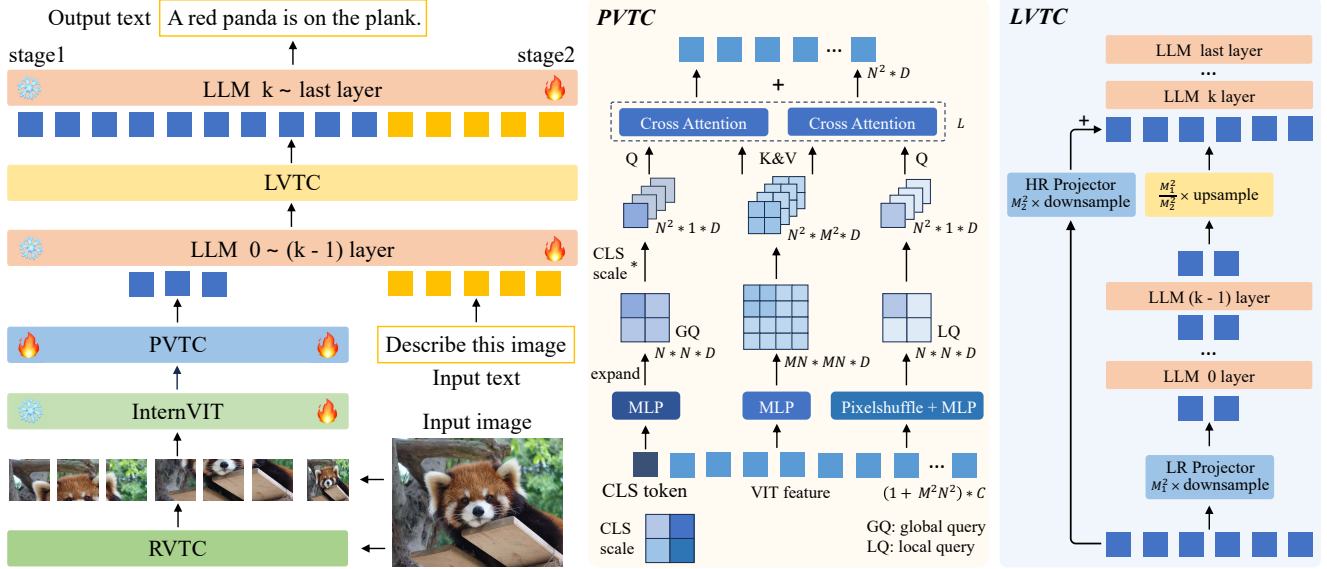


Figure 2. Architecture of the proposed InternVL-X incorporates three components: PVTC, LVTC, and RVTC. PVTC employs dual cross-attention on local and global queries to efficiently compress tokens. LVTC initially compresses visual tokens and subsequently expands them to improve their utilization across different LLM layers. RVTC optimizes image slicing to reduce the visual tokens numbers.

poses a multi-stage compression method and compresses visual tokens by considering both mean and maximum attention received from text tokens. Other approaches, such as TG-Llava [49] and Focus-Llava [57], also implement text-guided visual token compression methodologies.

### 2.3. High resolution

High resolution is crucial for the performance of MLLMs, and many works propose their processing methods. LLaVA-NeXT [33] splits high resolution images into a grid of patches with various configurations, encodes each independently, and then merges them into a long sequence alongside the global token. Monkey [29] incorporates a shared LoRA [20] structure within the visual encoder to accommodate various sub-images. SliME [55] utilizes adaptive slicing to scale input resolution and extracts contextual information from the global view using a mixture of adapters. Mini-Gemini-HD [28] employs dual encoders: the low resolution generates visual queries, while the high resolution provides keys and values, utilizing attention for enhanced fine-grained feature extraction. InternVL [7] and Internlm-Xcomposer2-4KHD [13] further expands the dynamic multi-resolution range, supporting up to 4K HD images, significantly improves performance.

## 3. Method

**Overview.** In this section, we first introduce the main bottlenecks of current MLLMs, and then present our method.

More visual tokens provide richer visual information and significantly improve the model performance, but due to the  $n^2$  complexity of the transformer [46] model, a large

number of visual tokens cause explosive growth in computational complexity. During the forward process of the MLLM, visual tokens typically exceed text tokens by over tenfold, which seriously affects the training efficiency. Balancing the performance and efficiency of MLLMs is an urgent issue that needs to be addressed.

In this work, we introduce InternVL-X, an enhanced version of the InternVL model. The architecture of InternVL-X, depicted in Fig. 2, comprises a visual encoder, a projector, and an LLM. Given an image  $V \in R^{H*W*3}$ , the visual encoder transforms it into CLS token  $F_{CLS} \in R^{1*C}$  and a set of visual embeddings  $F_V \in R^{S^2*C}$ . The projector then scales down  $F_V$  by a factor of  $M^2$  to produce the compressed visual token  $F_C \in R^{N^2*D}$ , where  $N = S/M$ . Finally, we concatenate  $F_C$  with text token  $F_T$  and feed them into the LLM to generate the output via an autoregressive paradigm. Please note that in this paper, unless otherwise specified, all  $\times$  symbols represent multiples and all  $*$  symbols represent multiplications.

We mainly compress visual tokens from the model and data perspectives. At the model level, we propose a new projector PVTC and an LLM compression module LVTC. PVTC serves as a bridge between the visual encoder and LLM, effectively converting visual features through global and local cross-attention mechanism. LVTC utilizes fewer visual tokens in the early LLM layers and only increases the tokens in the last few layers to enhance efficiency. At the data level, we design a high resolution slicing method RVTC, which reduces the number of slices by filtering the image area or edge length. Next, we will introduce each module separately.

### 3.1. PVTC

Existing projector token compression methods, like InternVL and MobileVLM, utilize pixel-shuffle or convolutional architectures to reduce visual tokens, often sacrificing critical local details in the process. TokenPacker partially addresses this limitation by employing cross-attention with downsampled local queries, but it neglects the global semantic information.

To address this, we propose PVTC, which leverages cross-attention mechanisms between visual tokens and dual queries—derived from local windows and the global CLS token, enabling efficient visual compression while preserving both fine-grained local details and comprehensive global semantics.

Specifically, our approach begins by recovering the spatial organization of visual embeddings from the final visual encoder layer. We first reshape the flattened visual embeddings  $F_V \in R^{S^2 * C}$  back into their original 2D spatial structure  $F_V \in R^{S * S * C}$ . These embeddings are then partitioned into non-overlapping  $N * N$  windows, each with  $M * M$  tokens, where  $M = 2^i, i \in [0, \log_2 S]$ . Within each window, we employ two parallel paths to generate the final compressed visual embeddings.

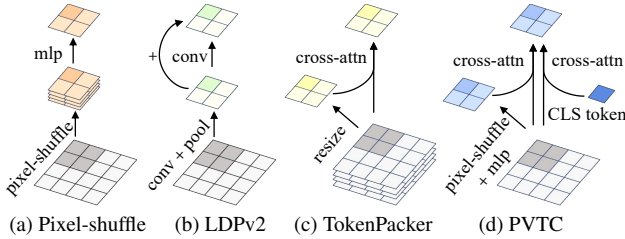


Figure 3. Comparison of different projectors.

**Local Attention.** For all visual tokens within a window, we compress them into 1 token through a pixel-shuffle operation, which transposes the  $M^2$  tokens in each window from the spatial to feature dimension. These compressed  $N * N$  tokens are then transformed through an MLP layer to match the feature dimension of the LLM, generating the local embedding  $F_{LQ} \in R^{N * N * D}$ . Subsequently, we convert the original visual embedding  $F_V$  to the same feature dimension to obtain  $F_{KV} \in R^{S * S * D}$ .  $F_{LQ}$  serves as the local query in cross-attention while  $F_{KV}$  acts as key and value. To reduce the amount of computation, we adopt the point-to-region cross-attention in [26], where each query only calculates the attention within its corresponding window. We accomplish this through a dimensionality transformation, and get  $F_{LQ} \in R^{N^2 * 1 * D}$ ,  $F_{KV} \in R^{N^2 * M^2 * D}$ . By applying cross-attention to each window, we produce compressed token  $F_L \in R^{N * N * D}$ , which enhances the retention and integration of local embeddings.

**Global Attention.** We utilize the CLS token as the global query, which aggregates the global information of

the image and could effectively extract the important information. We first transform the feature dimension of  $F_{CLS}$  from  $C$  to  $D$  through an MLP layer, and then expand it to 2D space to get  $F_{GQ} \in R^{N * N * D}$ . To avoid extracting much redundant information from similar tokens, we introduce diverse transformations to  $F_{GQ}$  at each position. Specifically, we set a learnable scale vector  $CLS\ scale \in R^{N * N * D}$ , which is multiplied by  $F_{GQ}$  to obtain a diverse global query. Similarly,  $F_{GQ}$  interacts with  $F_{KV}$  in each window separately. Through this process, we get global compressed embeddings  $F_G \in R^{N * N * D}$ , effectively capturing the overall semantic information.

After extracting features through  $L$  layers of attention, we combine  $F_L$  and  $F_G$  through element-wise addition and then reshape the result back into a 1D format to obtain the final compressed embeddings  $F_C \in R^{N^2 * D}$ . This combined representation retains both localized spatial details and comprehensive contextual information, achieving efficient compression while mitigating information loss.

### 3.2. LVTC

Previous studies, such as FastV and LLaVA-Mini, observe that most visual tokens receive high attention in the early layers of LLM, with this attention decreasing in deeper layers. However, the InternVL model demonstrates the opposite behavior. Our analysis, shown in Fig. 4, reveals that in the initial layers, both visual and text tokens mainly focus on their adjacent areas. As the model progresses to the deeper layers, the attention distance gradually increases. In the middle layers, only about 1/3 the visual tokens are activated by text tokens. In the final layers, most tokens gain high attention, peaking in the last layer. This suggests that in the early stages, attention is primarily distance-based. Consequently, numerous visual tokens in the early layers of LLM may not enhance performance and could undermine computational efficiency.

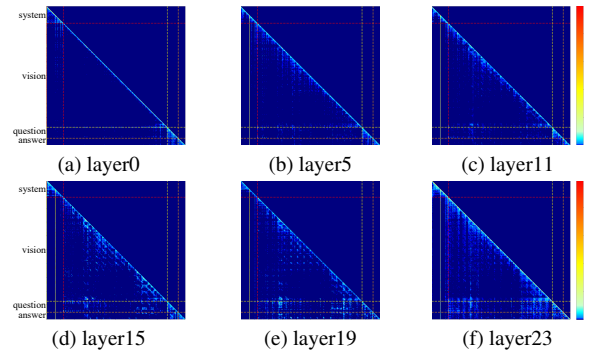


Figure 4. Visualization of average attention weights of each token in the LLM process. The horizontal axis is the key position and the vertical axis is the query position.

Building on the above observations, we design a layer-wise visual token compression module LVTC. Unlike most

previous methods that progressively compress tokens layer by layer, our approach compresses tokens right at the input layer and increase tokens at a specific layer  $k$ . During the forward pass of LLM, the token presents a “T” shape, as illustrated in Fig. 5. In detail, we first perform a low resolution (LR) compression, leveraging an LR projector to compress  $F_V$  by a factor of  $M_1^2$ , thus obtaining  $N_1^2$  tokens, where  $M_1 = S/N_1$ . Then we calculate attention on these  $N_1^2$  tokens in the first  $k$  layers of LLM. At layer  $k$ , we expand the token count to  $N_2^2$  through an Upsample2D process, with an upsampling scale factor of  $M_1^2/M_2^2$ , where  $M_2 = S/N_2$ ,  $M_1 > M_2$  and  $N_2 \gg N_1$ . This methodology allows most computations to focus on the reduced set of  $N_1^2$  tokens across most layers, only increases to  $N_2^2$  tokens in the final layers. Compared to using  $N_2^2$  tokens throughout all layers, our approach maintains identical performance while significantly decreasing computational demands.

### Algorithm 1 LVTC

```

# V: Visual token, T: Text token, s: insert start layer, i: insert interval,
k: token expansion layer, vis_pos: position of visual token, LRProjs,
HRProj, VLR, VHR
for proj in LRProjs do
  VLR.append(proj(V))
VHR = HRProj(V)
X = concat(VLR[0], T); del VLR[0]
for idx, layer in enumerate(LLM.layers) do
  if idx == k then
    X = concat(upsample2d(X[vis_pos]) + VHR, X[!vis_pos])
  else if s <= idx < s + i * len(VLR) and (idx - s) % i == 0 then
    X[vis_pos] += VLR[(idx - s) // i]
X = layer(X)

```

Although LVTC expands visual tokens in deep layers, the upsampling operation does not bring more visual information. Inspired by ResNet [19] and FPN [31], we introduce an additional high resolution (HR, different from the concept in Sec. 2.3) compression that converts  $F_V$  into  $N_2^2$  tokens through a HR projector. These tokens are then integrated with the upsampled  $N_2^2$  tokens at layer  $k$  through residual connections. This approach effectively injects visual information into the LLM without loss. To further diversify the visual input and mitigate the risk of visual knowledge forgetting, we incorporate a multi-projector strategy into the middle layers of LLM through residual connections. Specifically, we set  $T$  LR projectors to obtain  $T$  groups of compressed tokens. Beginning at the  $s - th$  layer of LLM, we integrate a set of compressed tokens into the visual tokens at intervals of  $i$  layers. The LVTC structure and computational process are shown in Fig. 5 and Alg. 1, which enhances the model’s capacity to retain and utilize visual information effectively.

### 3.3. RVTC

Several models, like LLaVA-NeXT and InternVL, use high resolution strategy to enhance performance. However, this

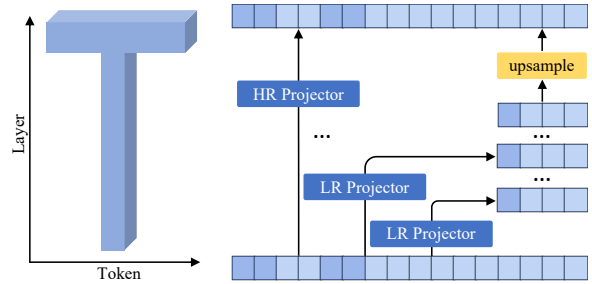


Figure 5. LVTC uses a high resolution projector and multi-projector structure to enhance visual information in LLM.

approach leads to a significant increase in visual tokens and computational demands. For instance, setting the number of slices to 4 will result in a  $2.5\times$  increase in training time. InternVL predefines several aspect ratios and determines the number of slices by matching the optimal ratio. Although effective, this method can cause computational inefficiencies, particularly when processing small images with large aspect ratios. To illustrate, if the maximum number of patches is set to 6, an  $80 \times 20$  image will be assigned a 4:1 ratio and divided into 4 patches, while a  $345 \times 372$  image fits best with a 1:1 ratio and remains unsliced. This ratio matching mechanism results in an uneven distribution of computational resources, significantly affecting training efficiency.

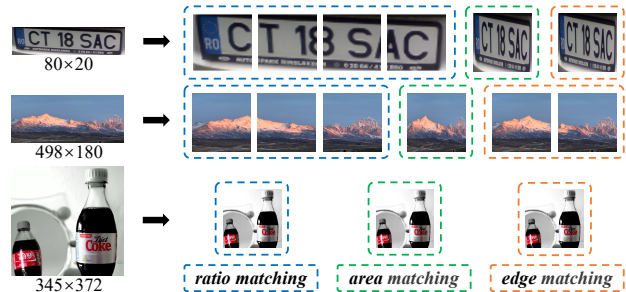


Figure 6. Different slicing methods. Compared to ratio matching, area matching and edge matching require fewer slices.

To tackle this issue, we introduce an efficient image slicing method RVTC. The amount of information an image is largely determined by its pixel count. Building on this principle, we propose two innovative matching strategies: area matching and edge length matching. Consider an image with a resolution of  $(W, H)$ , and an input resolution for the MLLM set at  $(448, 448)$ , along with a predefined maximum number of patches  $R = 6$ . In the area matching method, we take  $448 \times 448$  as a basic unit to determine the maximum number of slices. Specifically, we first compute  $R = \min(R, \lceil W * H / (448 * 448) \rceil)$ , then execute the optimal match. Similarly, in the edge length matching method, we utilize the side length as the measurement unit to calculate  $R$ . In this case,  $R = \min(R, R_W * R_H)$ , where  $R_W = \lceil W / 448 \rceil$ ,  $R_H = \lceil H / 448 \rceil$ . Fig. 6 il-

Model	LLM	PT/IT	Token	Text-oriented VQA				General VQA			Comprehensive benchmark					Avg	
				Text VQA	Doc VQA	Chart QA	Info VQA	GQA	VQA v2	Viz Wiz	MMB	MM Vet	MM MU	PO PE	SEED -IMG		
MobileVLM V2[10]	Mobilellama-2.7B	1.2M/3.6M	144	52.1	-	-	-	59.3	-	-	-	-	-	-	84.3	-	-
BLIP-2[25]	Vicuna-13B	129M/-	32	42.5	-	-	-	41.0	65.0	19.6	-	-	-	-	85.3	49.7	-
Insturct-BLIP[11]	Vicuna-7B	129M/1.2M	64	50.1	-	-	-	49.5	-	34.5	-	26.3	-	-	-	-	-
QwenVL[2]	Qwen-7B	1.4B/50M	256	63.8	65.1*	65.7*	-	59.3*	78.8*	35.2	-	-	-	-	-	62.3	-
VILA[30]	Llama2-7B	50M/1M	576	64.4	-	58.6*	-	62.3*	79.9*	57.8	68.9	34.9	-	-	85.5	-	-
MobileVLM V2[10]	Vicuna-7B	1.2M/3.6M	144	62.3	-	-	-	62.6	-	-	-	-	-	-	85.3	-	-
MiniGemini[28]	Vicuna-7B	1.2M/1.5M	576	65.9	-	-	-	-	-	-	68.5	46.0	38.1	-	-	-	-
LLaVA-1.5[32]	Vicuna-7B	558K/665K	576	58.2	28.1	-	25.8	63.3*	78.5*	50.0	64.3	31.1	35.3	85.9	66.1	-	-
TokenPacker[26]	Vicuna-7B	558K/665K	144	-	-	-	-	61.9*	77.9*	52.0	65.1	33.0	-	-	87.0	-	-
InternVL2[7]#	Internlm2-1.8B	558K/665K	256	44.99	23.21	14.23	16.56	61.03*	74.20*	47.55	59.75	24.6	29.7	86.33	64.48	-	45.47
InternVL2[7]#	Internlm2.5-7B	558K/665K	256	49.73	26.94	18.08	21.82	63.01*	77.79*	50.56	70.85	34.1	39.2	86.78	71.13	-	50.83
InternVL-X	Internlm2-1.8B	558K/665K	256	49.91	27.31	19.03	17.71	61.55	74.86*	51.83	63.34	28.6	32.2	86.21	65.39	-	48.32
InternVL-X	Internlm2.5-7B	558K/665K	256	55.24	31.72	21.83	23.90	63.62	78.69*	54.51	72.64	41.7	41.9	87.13	72.58	-	53.85
Monkey[29]	Qwen-7B	-/1.44M	~1024	67.7	66.5	36.1	-	60.7	80.3*	61.2	-	-	-	-	-	-	-
TokenPacker-HD[26]	Vicuna-7B	1.2M/1.5M	~954	68.0	60.2	-	-	-	81.2*	54.7	67.4	-	35.4	-	-	-	-
Mini-Gemini-HD[28]	Vicuna-7B	1.2M/1.5M	2880	68.4	65.0	-	-	-	80.3*	54.6	65.8	41.3	36.8	86.8	-	-	-
LLaVA-UHD[16]	Vicuna-13B	595K/665K	~256	67.7	-	-	-	-	81.7*	56.1	-	-	-	89.1	-	-	-
LLaVA-NeXT[33]	Vicuna-7B	558K/765K	~2880	64.9	74.4	54.8	37.1	64.2	81.8*	57.6	68.1	43.9	35.8	86.5	68.2	-	61.38
InternVL2-HD[7]#	Internlm2-1.8B	558K/770K	~1282	59.59	66.60*	62.80*	25.69	60.24*	75.60*	51.24	62.50	27.6	29.1	87.36	66.93	-	56.27
InternVL2-HD[7]#	Internlm2.5-7B	558K/770K	~1282	65.58	72.64*	69.77*	30.87	63.24*	78.85*	56.33	72.08	35.7	39.9	87.25	73.42	-	62.13
InternVL-X-HD	Internlm2-1.8B	558K/770K	~520	63.32	69.22*	64.48*	28.75	61.35*	76.52*	57.24	63.67	30.8	33.2	87.25	67.72	-	58.64
InternVL-X-HD	Internlm2.5-7B	558K/770K	~520	68.56	75.81*	73.24*	38.05	63.50*	79.61*	56.27	74.66	40.7	42.1	86.95	74.23	-	64.47

Table 1. Comparison of Different Methods on 12 benchmarks. \* indicates that the training set of this benchmark is visible during the model training. # means that the model is not an official checkpoint, but our reproduced version.

illustrates a comparison of different slicing methods, highlighting the completeness and efficiency of RVTC in image slicing. This strategy maximizes the utilization of available pixels, thereby enhancing the efficiency of model training.

## 4. Experiments

This section presents our experimental setup and results. We first describe our model training specifications, followed by evaluation benchmarks and datasets. We then compare our model’s performance with existing methods and conclude with ablation studies on the proposed methods.

### 4.1. Implement details and datasets

**Experiments configuration.** We initialize InternVL-X models with the same pre-trained components as the InternVL2 series. For the 2B model, we employ InternViT-300M-448px [8] as the visual encoder and InternLM2-Chat-1.8B [3] as the LLM, while the 8B variant uses the same visual encoder but upgrades to InternLM2.5-Chat-7B [43] for LLM. Our training strategy follows a two-stage approach similar to LLaVA-1.5. In the pretraining stage, we finetune only the projector module and freeze other parameters, followed by an instruction tuning stage where all model parameters are finetuned. All models are trained for 1 epoch using the AdamW optimizer with a cosine learning rate scheduler. The initial learning rate is set to 4e-5. The training is conducted on 8 NVIDIA A800 GPUs. In normal resolution experiments, we use PVTC and LVTC, and in high resolution, we adopt PVTC, LVTC, and RVTC.

**Training datasets.** We follow the training datasets as LLaVA-1.5 and LLaVA-NeXT. In the first stage, we utilize LCS-558K [34] dataset to finetune the projector. In the second stage, for normal resolution model, we use LLaVA-665K [34] dataset for instruction tuning. For high resolution model, as the dataset used in LLaVA-NeXT is not publicly available, we assemble an instruction tuning dataset with 770K samples following the guidance of LLaVA-NeXT.

**Evaluation benchmarks.** For fair evaluation, we assess our model on 12 diverse benchmarks, which span text-oriented VQA (TextVQA [44], DocVQA [39], ChartQA [38], InfoVQA [40]), general VQA (GQA [21], VQAv2 [15], VizWiz [17]), and comprehensive evaluation (MMB [36], MMVet [50], MMMU [51], POPE [27], SEED [22]).

### 4.2. Quantitive results

We conduct comprehensive evaluations of our InternVL-X series models across 12 benchmarks. To ensure fair comparison, we implement InternVL2 by training the official InternVL2 architecture from scratch, using the same training data and initialization as our InternVL-X, rather than using the official InternVL2 checkpoints. As shown in Tab. 1, compared with InternVL2, the 2B and 8B versions of InternVL-X improve the average performance by 2.85% and 3.02% across all 12 benchmarks, respectively. With high resolution, InternVL-X improves these two metrics by 2.37% and 2.34%. Furthermore, InternVL-X-8B achieves the state-of-the-art results on 7 benchmarks. Using less than 20% of the tokens, we exceed the average performance of LLaVA-NeXT by 2.34%.

**Text-oriented VQA.** We evaluate InternVL-X against other models across 4 challenging benchmarks. Our 2B and 8B models demonstrate an average improvement of 4.22% and 4.23%, respectively, over the baseline model InternVL2. Notably, some tasks like DocVQA are zero-shot evaluations. Our 8B version achieves best result on the DocVQA task. In the TextVQA and InfoVQA tasks, despite our models showing considerable improvements, there remains a gap between our model and those of SOTA models like LLaVA-1.5. In high resolution evaluation, more training data and finer-grained visual information lead to substantial improvements. Impressively, the InternVL-X-8B achieves the best results in all of the 4 tasks.

**General VQA.** We conduct an evaluation on 3 classic tasks: VQAv2, GQA, and VizWiz. As presented in Tab. 1, InternVL-X surpasses the baseline model across all 3 tasks, enhancing the average metric by 2.15% and 1.82%. Our model excels particularly on the GQA task, achieving the best performance. While our approach slightly lags behind the leading models on the VQAv2 and VizWiz tasks, it still delivers competitive results.

**Comprehensive benchmark.** Our approach demonstrates exceptional performance across the MMB, MMMU, and SEED-IMG benchmarks. In high resolution evaluations, InternVL-X surpasses LLaVA-NeXT, improving the MMB and MMMU metrics by 6.56% and 6.3%, respectively. Unfortunately, our method is slightly inferior to the baseline on the hallucination benchmark POPE. We speculate that richer visual information may increase the probability of hallucination in the model. Impressively, our 2B model could achieve comparable results to other 7B models in certain metrics, showcasing the outstanding performance of InternVL-X on visual benchmarks.

### 4.3. Ablation study

We conduct sufficient ablation experiments on our proposed method using the InternVL2 model as the base model. If there is no special explanation, the following ablation experiments are all conducted on the 2B model with normal resolution. We report the performance on 6 benchmarks, including TextVQA, DocVQA, GQA, VizWiz, MMVet and POPE. Next, we will introduce each part in detail.

We explore the complementary interactions among our three proposed modules and their individual impacts on models, as illustrated in Tab. 2. PVTC alone improves the model’s performance by 2.25% across 6 benchmarks. With more visual information, LVTC could also significantly improve the model effect, and it could bring superposition of effects with PVTC. However, as LVTC has not yet been implemented on flash attention [12], it has somewhat increased the training time. Nevertheless, compared to the baseline experiment without flash attention and token compression, LVTC demonstrates notable enhancements in

Method	Token	Accuracy	Train/Inference Time
Base	256	47.78	4.1h/39.9ms
Base*	1024	49.93	11.1h/40.6ms
Base-HD	~1282	58.77	13.5h/46.7ms
+ PVTC	256	50.03	4.3h/42.7ms
+ LVTC*	256	50.26	7.0h/40.3ms
+ PVTC + LVTC*	256	50.90	7.3h/41.6ms
+ RVTC	~520	58.21	8.6h/43.3ms
+ PVTC + RVTC	~520	60.85	9.1h/44.5ms
Full Model*	~520	61.56	18.7h/45.2ms

Table 2. Ablation study of different components. \* indicates that flash attention is not used. The training time in the table is the sum of PT and IT time, and the inference time is the average generation latency of per token.

both performance and efficiency. Although RVTC slightly diminishes model performance, it achieves considerable reductions in training time. Moreover, when all three modules are combined into a single model, both performance and efficiency exceed those of models utilizing individual modules, underscoring the complementary nature of our proposed modules. Additionally, since kv-cache is used to accelerate the inference process, we find that the impact of token length on inference time is almost negligible.

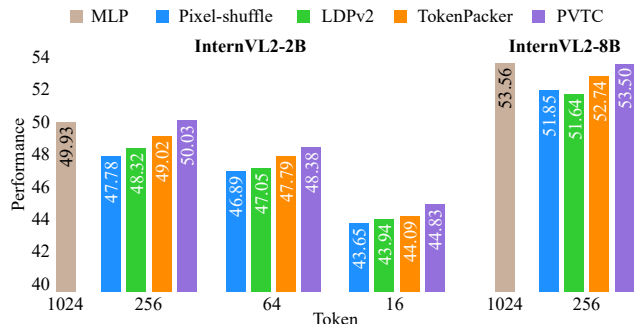


Figure 7. Comparison of various projectors under different compression ratios.

**PVTC.** To validate the effectiveness of our proposed PVTC module, we compare PVTC with other projectors, including Pixel-shuffle [8], LDPv2 [10], and TokenPacker [26]. For a fair comparison, we utilize different projectors on InternVL2 to replace the original projector, and all methods are trained with the same training data and experimental settings. We first perform linear projector(MLP) [32] to assess model performance without token compression (1024 token). Subsequently, we conduct experiments with various projectors under 4×, 16×, and 64× compression ratios (corresponding to 256, 64, and 16 tokens, respectively). As shown in Fig. 7, PVTC consistently outperforms alternative methods across all compression ratios. At 256 tokens, our method enhances the performance over Pixel-shuffle, LDPv2, and TokenPacker by 2.25%, 1.71%, and 1.01%, respectively, and achieves results comparable to

Method	Global Attn	Local Attn	Text VQA	Doc VQA	GQA	Viz Wiz	MM Vet	PO PE	Avg
Base	0	0	44.99	23.21	61.03	46.55	24.6	86.33	47.78
PVTC	1	0	44.52	22.57	60.52	47.13	23.1	85.31	47.19
	1*	0	45.33	22.98	61.35	48.79	25.4	86.21	48.34
	0	1	45.76	23.44	61.64	51.33	26.8	86.98	49.32
	1*	1	47.69	24.82	61.81	51.41	27.8	86.67	50.03
	2*	2	47.92	25.11	61.63	52.33	27.6	87.21	50.30
	3*	3	47.51	24.76	60.97	49.88	27.9	87.03	49.67

Table 3. Ablation experiments on global attention and local attention. \* indicates that use learnable CLS scale.

the linear projector, reaching the performance limit without token compression. We attribute this to PVTC’s dual-query design, which allows the compressed visual tokens to effectively capture global semantics and local details.

To further understand the individual contributions of each component in PVTC, we perform an ablation study focusing on local and global queries, particularly examining the effect of different attention layers  $L$  on the results. When both layers are set to 0, this configuration corresponds to the baseline setup of InternVL2. As indicated in Table 3, utilizing either query type alone enhances performance compared to the baseline model, while combining both queries achieves the best performance. When using only the CLS token for querying, the model experiences limited improvements, while introducing learnable CLS scales significantly boosts the performance of global query. These results demonstrate that local and global queries offer complementary advantages, each capturing distinct aspects of visual information. We find that PVTC performs optimally with 1~2 layers. The performance tends to decline when  $L > 2$ . To balance the parameters and performance, we ultimately set  $L = 1$ .

**LVTC.** We set  $M_1 = 2$  (corresponding to 256 tokens),  $M_2 = 1$  (corresponding to 1024 tokens) and  $k$  as the  $3/4$  layer of LLM, where  $k = 17$  for 2B model and  $k = 23$  for 8B model. We adopt the Pixel-shuffle + MLP as basic projector. For base model, we conduct experiments under 3 distinct compression settings: LR compression (256), HR compression (1024), and HR→LR compression (1024→256). For LVTC, we initially apply LR compression and expand it to HR compression at layer  $k$ . Additionally, we assess the impact of the HR projector and multi-projector components. The experimental findings, summarized in Table 4, lead to three conclusions: 1. The model’s performance is mainly influenced by the token numbers, with more tokens generally yielding better results. 2. Backward compression is more effective than forward compression, indicating that visual tokens primarily contribute in deeper layers. 3. Upsampling to increase tokens doesn’t enhance performance, while integrating information from HR projector and multi-projector significantly boosts it. In the 2B model, these two modules individually contribute per-

formance improvements of 1.87% and 0.98%, respectively, while their combined effect brings a total gain of 2.32%, exceeding the performance without token compression.

Model	Method	Token $0 \sim k-1$	Token $k \sim last$	HR proj	Multi proj	Accuracy
InternVL2-2B	Base	256	256			47.78
		1024	1024			49.93
		1024	256			48.05
InternVL2-2B	LVTC	256	1024			47.91
		256	1024	✓		49.78
		256	1024		✓	48.89
		256	1024	✓	✓	50.23
InternVL2-8B	Base	256	256			51.85
		1024	1024			53.56
	LVTC	256	1024	✓		53.38
		256	1024	✓	✓	53.77

Table 4. Component-wise ablation study of LVTC.

Furthermore, we explore the impact of parameters  $M_1$ ,  $M_2$ , and  $k$ . As illustrated in Fig. 8, the performance upper limit and computational bottleneck of the model are primarily influenced by  $M_2$ . Increasing  $M_1$  will lead to performance degradation. With setting  $M_1 = 2$ ,  $M_2 = 1$ , as  $k$  decreases from 1 to  $3/4$ , the model’s performance demonstrates an almost linear improvement. Afterwards, the metrics slightly increase and then stabilize. When  $k$  reaches  $1/2$ , the performance becomes essentially saturated.

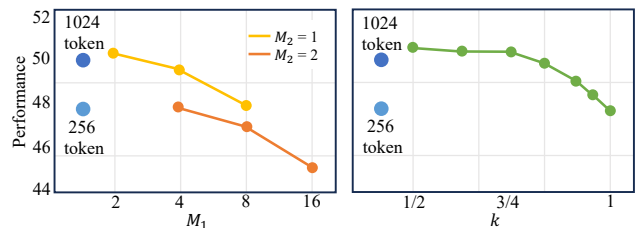


Figure 8. Ablation experiments on, left: LR compression and HR compression multiples, right: token expansion layer.

**RVTC.** We utilize various image slicing methods for verification, with a dataset of 770K training samples and a maximum patch size set to 6. We compare the average number of patches, average token, training time, and performance across ratio matching, area matching, and edge length matching methods, as shown in Table 5. Compared to the baseline method, the area matching and edge length matching strategies on the 2B model require only 49.62% and 58.51% of the training time, respectively, while achieving 97.77% and 99.04% of the performance of the ratio matching method. The conclusions on the 8B model are similar, with just 50.69% and 59.88% of the training time, our methods could reach 97.98% and 99.26% of the baseline model’s performance, respectively. By maximizing the utilization of visual information, our proposed method significantly enhances model training efficiency with slight performance loss.

Model	Method	Average patch	Average token	Train time	Accuracy
InternVL2-2B	Base-ratio	5.009	1282	13.5h	58.77
	RVTC-area	1.559	399	6.7h	57.46
	RVTC-edge	2.033	520	7.9h	58.21
InternVL2-8B	Base-ratio	5.009	1282	35.9h	63.45
	RVTC-area	1.559	399	18.2h	62.17
	RVTC-edge	2.033	520	21.5h	62.98

Table 5. Experimental comparison of different slicing methods.

## 5. Conclusion

This paper presents the InternVL-X series, showcasing three innovative visual token compression modules: PVTC, LVTC, and RVTC. These modules significantly enhance model effectiveness and training optimization. PVTC employs a grid-based cross-attention approach to effectively balance local detail with global semantics. LVTC compresses tokens early and expand them in deep layers to enhance LLM efficiency. Meanwhile, RVTC optimizes high resolution image slicing based on pixel counts or edge length, thereby boosting training speed with minimal impact on performance. Overall, InternVL-X models achieve state-of-the-art results across multiple benchmarks, outperforming other open-source models and delivering substantial improvements in both performance and efficiency.

## References

- [1] Jean-Baptiste Alayrac, Jeff Donahue, Pauline Luc, Antoine Miech, Iain Barr, Yana Hasson, Karel Lenc, Arthur Mensch, Katherine Millican, Malcolm Reynolds, et al. Flamingo: a visual language model for few-shot learning. *Advances in neural information processing systems*, 35:23716–23736, 2022. [2](#)
- [2] Jinze Bai, Shuai Bai, Shusheng Yang, Shijie Wang, Sinan Tan, Peng Wang, Junyang Lin, Chang Zhou, and Jingren Zhou. Qwen-vl: A frontier large vision-language model with versatile abilities. *arXiv preprint arXiv:2308.12966*, 2023. [1](#), [2](#), [6](#)
- [3] Zheng Cai, Maosong Cao, Haojiong Chen, Kai Chen, Keyu Chen, Xin Chen, Xun Chen, Zehui Chen, Zhi Chen, Pei Chu, et al. Internlm2 technical report. *arXiv preprint arXiv:2403.17297*, 2024. [6](#)
- [4] Junbum Cha, Wooyoung Kang, Jonghwan Mun, and Byungseok Roh. Honeybee: Locality-enhanced projector for multimodal llm. In *Proceedings of the IEEE/CVF Conference on Computer Vision and Pattern Recognition*, pages 13817–13827, 2024. [2](#)
- [5] Lin Chen, Jinsong Li, Xiaoyi Dong, Pan Zhang, Conghui He, Jiaqi Wang, Feng Zhao, and Dahua Lin. Sharegpt4v: Improving large multi-modal models with better captions. In *European Conference on Computer Vision*, pages 370–387. Springer, 2024. [2](#)
- [6] Liang Chen, Haozhe Zhao, Tianyu Liu, Shuai Bai, Junyang Lin, Chang Zhou, and Baobao Chang. An image is worth 1/2 tokens after layer 2: Plug-and-play inference acceleration for large vision-language models. In *European Conference on Computer Vision*, pages 19–35. Springer, 2025. [2](#)
- [7] Zhe Chen, Weiyun Wang, Hao Tian, Shenglong Ye, Zhangwei Gao, Erfei Cui, Wenwen Tong, Kongzhi Hu, Jiapeng Luo, Zheng Ma, et al. How far are we to gpt-4v? closing the gap to commercial multimodal models with open-source suites. *arXiv preprint arXiv:2404.16821*, 2024. [1](#), [2](#), [3](#), [6](#)
- [8] Zhe Chen, Jiannan Wu, Wenhai Wang, Weijie Su, Guo Chen, Sen Xing, Muyan Zhong, Qinglong Zhang, Xizhou Zhu, Lewei Lu, et al. Internvl: Scaling up vision foundation models and aligning for generic visual-linguistic tasks. In *Proceedings of the IEEE/CVF Conference on Computer Vision and Pattern Recognition*, pages 24185–24198, 2024. [1](#), [2](#), [6](#), [7](#)
- [9] Xiangxiang Chu, Limeng Qiao, Xinyang Lin, Shuang Xu, Yang Yang, Yiming Hu, Fei Wei, Xinyu Zhang, Bo Zhang, Xiaolin Wei, et al. Mobilevlm: A fast, strong and open vision language assistant for mobile devices. *arXiv preprint arXiv:2312.16886*, 2023. [2](#)
- [10] Xiangxiang Chu, Limeng Qiao, Xinyu Zhang, Shuang Xu, Fei Wei, Yang Yang, Xiaofei Sun, Yiming Hu, Xinyang Lin, Bo Zhang, et al. Mobilevlm v2: Faster and stronger baseline for vision language model. *arXiv preprint arXiv:2402.03766*, 2024. [2](#), [6](#), [7](#)
- [11] Wenliang Dai, Junnan Li, Dongxu Li, Anthony Meng Huat Tiong, Junqi Zhao, Weisheng Wang, Boyang Li, Pascale Fung, and Steven Hoi. Instructblip: Towards general-purpose vision-language models with instruction tuning, 2023. [1](#), [2](#), [6](#)
- [12] Tri Dao, Dan Fu, Stefano Ermon, Atri Rudra, and Christopher Ré. Flashattention: Fast and memory-efficient exact attention with io-awareness. *Advances in neural information processing systems*, 35:16344–16359, 2022. [7](#)
- [13] Xiaoyi Dong, Pan Zhang, Yuhang Zang, Yuhang Cao, Bin Wang, Linke Ouyang, Songyang Zhang, Haodong Duan, Wenwei Zhang, Yining Li, et al. Internlm-xcomposer2-4khd: A pioneering large vision-language model handling resolutions from 336 pixels to 4k hd. *Advances in Neural Information Processing Systems*, 37:42566–42592, 2025. [3](#)
- [14] Alexey Dosovitskiy, Lucas Beyer, Alexander Kolesnikov, Dirk Weissenborn, Xiaohua Zhai, Thomas Unterthiner, Mostafa Dehghani, Matthias Minderer, Georg Heigold, Sylvain Gelly, et al. An image is worth 16x16 words: Transformers for image recognition at scale. *arXiv preprint arXiv:2010.11929*, 2020. [1](#)
- [15] Yash Goyal, Tejas Khot, Douglas Summers-Stay, Dhruv Batra, and Devi Parikh. Making the v in vqa matter: Elevating the role of image understanding in visual question answering. In *Proceedings of the IEEE conference on computer vision and pattern recognition*, pages 6904–6913, 2017. [6](#)
- [16] Zonghao Guo, Ruyi Xu, Yuan Yao, Junbo Cui, Zanlin Ni, Chunjiang Ge, Tat-Seng Chua, Zhiyuan Liu, and Gao Huang. Llava-uhd: an lmm perceiving any aspect ratio and high resolution images. In *European Conference on Computer Vision*, pages 390–406. Springer, 2024. [6](#)
- [17] Danna Gurari, Qing Li, Abigale J Stangl, Anhong Guo, Chi Lin, Kristen Grauman, Jiebo Luo, and Jeffrey P Bigham.

- Vizwiz grand challenge: Answering visual questions from blind people. In *Proceedings of the IEEE conference on computer vision and pattern recognition*, pages 3608–3617, 2018. 6
- [18] Yuhang Han, Xuyang Liu, Pengxiang Ding, Donglin Wang, Honggang Chen, Qingsen Yan, and Siteng Huang. Rethinking token reduction in mllms: Towards a unified paradigm for training-free acceleration. *arXiv preprint arXiv:2411.17686*, 2024. 2
- [19] Kaiming He, Xiangyu Zhang, Shaoqing Ren, and Jian Sun. Deep residual learning for image recognition. In *Proceedings of the IEEE conference on computer vision and pattern recognition*, pages 770–778, 2016. 5
- [20] Edward J Hu, Yelong Shen, Phillip Wallis, Zeyuan Allen-Zhu, Yuanzhi Li, Shean Wang, Lu Wang, Weizhu Chen, et al. Lora: Low-rank adaptation of large language models. *ICLR*, 1(2):3, 2022. 3
- [21] Drew A Hudson and Christopher D Manning. Gqa: A new dataset for real-world visual reasoning and compositional question answering. In *Proceedings of the IEEE/CVF conference on computer vision and pattern recognition*, pages 6700–6709, 2019. 6
- [22] Bohao Li, Rui Wang, Guangzhi Wang, Yuying Ge, Yixiao Ge, and Ying Shan. Seed-bench: Benchmarking multimodal llms with generative comprehension. *arXiv preprint arXiv:2307.16125*, 2023. 6
- [23] Bo Li, Yuanhan Zhang, Dong Guo, Renrui Zhang, Feng Li, Hao Zhang, Kaichen Zhang, Peiyuan Zhang, Yanwei Li, Ziwei Liu, et al. Llava-onevision: Easy visual task transfer. *arXiv preprint arXiv:2408.03326*, 2024. 1, 2
- [24] Junnan Li, Dongxu Li, Caiming Xiong, and Steven Hoi. Blip: Bootstrapping language-image pre-training for unified vision-language understanding and generation. In *International conference on machine learning*, pages 12888–12900. PMLR, 2022. 1
- [25] Junnan Li, Dongxu Li, Silvio Savarese, and Steven Hoi. Blip-2: Bootstrapping language-image pre-training with frozen image encoders and large language models. In *International conference on machine learning*, pages 19730–19742. PMLR, 2023. 1, 2, 6
- [26] Wentong Li, Yuqian Yuan, Jian Liu, Dongqi Tang, Song Wang, Jie Qin, Jianke Zhu, and Lei Zhang. Tokenpacker: Efficient visual projector for multimodal llm. *arXiv preprint arXiv:2407.02392*, 2024. 2, 4, 6, 7
- [27] Yifan Li, Yifan Du, Kun Zhou, Jimpeng Wang, Wayne Xin Zhao, and Ji-Rong Wen. Evaluating object hallucination in large vision-language models. *arXiv preprint arXiv:2305.10355*, 2023. 6
- [28] Yanwei Li, Yuechen Zhang, Chengyao Wang, Zhisheng Zhong, Yixin Chen, Ruihang Chu, Shaoteng Liu, and Jiaya Jia. Mini-gemini: Mining the potential of multi-modality vision language models. *arXiv preprint arXiv:2403.18814*, 2024. 3, 6
- [29] Zhang Li, Biao Yang, Qiang Liu, Zhiyin Ma, Shuo Zhang, Jingxu Yang, Yabo Sun, Yuliang Liu, and Xiang Bai. Monkey: Image resolution and text label are important things for large multi-modal models. In *proceedings of the IEEE/CVF conference on computer vision and pattern recognition*, pages 26763–26773, 2024. 3, 6
- [30] Ji Lin, Hongxu Yin, Wei Ping, Pavlo Molchanov, Mohammad Shoeybi, and Song Han. Vila: On pre-training for visual language models. In *Proceedings of the IEEE/CVF conference on computer vision and pattern recognition*, pages 26689–26699, 2024. 2, 6
- [31] Tsung-Yi Lin, Piotr Dollár, Ross Girshick, Kaiming He, Bharath Hariharan, and Serge Belongie. Feature pyramid networks for object detection. In *Proceedings of the IEEE conference on computer vision and pattern recognition*, pages 2117–2125, 2017. 5
- [32] Haotian Liu, Chunyuan Li, Yuheng Li, and Yong Jae Lee. Improved baselines with visual instruction tuning. In *Proceedings of the IEEE/CVF Conference on Computer Vision and Pattern Recognition*, pages 26296–26306, 2024. 1, 2, 6, 7
- [33] Haotian Liu, Chunyuan Li, Yuheng Li, Bo Li, Yuanhan Zhang, Sheng Shen, and Yong Jae Lee. Llava-next: Improved reasoning, ocr, and world knowledge, 2024. 3, 6
- [34] Haotian Liu, Chunyuan Li, Qingyang Wu, and Yong Jae Lee. Visual instruction tuning. *Advances in neural information processing systems*, 36, 2024. 1, 2, 6
- [35] Ting Liu, Liangtao Shi, Richang Hong, Yue Hu, Quanjun Yin, and Linfeng Zhang. Multi-stage visual token dropping: Towards efficient multimodal large language model. *arXiv preprint arXiv:2411.10803*, 2024. 2
- [36] Yuan Liu, Haodong Duan, Yuanhan Zhang, Bo Li, Songyang Zhang, Wangbo Zhao, Yike Yuan, Jiaqi Wang, Conghui He, Ziwei Liu, et al. Mmbench: Is your multi-modal model an all-around player? In *European conference on computer vision*, pages 216–233. Springer, 2024. 6
- [37] Haoyu Lu, Wen Liu, Bo Zhang, Bingxuan Wang, Kai Dong, Bo Liu, Jingxiang Sun, Tongzheng Ren, Zhuoshu Li, Hao Yang, et al. Deepseek-vl: towards real-world vision-language understanding. *arXiv preprint arXiv:2403.05525*, 2024. 2
- [38] Ahmed Masry, Do Xuan Long, Jia Qing Tan, Shafiq Joty, and Enamul Hoque. Chartqa: A benchmark for question answering about charts with visual and logical reasoning. *arXiv preprint arXiv:2203.10244*, 2022. 6
- [39] Minesh Mathew, Dimosthenis Karatzas, and CV Jawahar. Docvqa: A dataset for vqa on document images. In *Proceedings of the IEEE/CVF winter conference on applications of computer vision*, pages 2200–2209, 2021. 6
- [40] Minesh Mathew, Viraj Bagal, Rubèn Tito, Dimosthenis Karatzas, Ernest Valveny, and CV Jawahar. Infographicvqa. In *Proceedings of the IEEE/CVF Winter Conference on Applications of Computer Vision*, pages 1697–1706, 2022. 6
- [41] Alec Radford, Jong Wook Kim, Chris Hallacy, Aditya Ramesh, Gabriel Goh, Sandhini Agarwal, Girish Sastry, Amanda Askell, Pamela Mishkin, Jack Clark, et al. Learning transferable visual models from natural language supervision. In *International conference on machine learning*, pages 8748–8763. PMLR, 2021. 2
- [42] Yuzhang Shang, Mu Cai, Bingxin Xu, Yong Jae Lee, and Yan Yan. Llava-prumerge: Adaptive token reduction for efficient

- large multimodal models. *arXiv preprint arXiv:2403.15388*, 2024. 2
- [43] ShanghaiAILab. Internlm. <https://github.com/InternLM/InternLM>, 2024. 6
- [44] Amanpreet Singh, Vivek Natarajan, Meet Shah, Yu Jiang, Xinlei Chen, Dhruv Batra, Devi Parikh, and Marcus Rohrbach. Towards vqa models that can read. In *Proceedings of the IEEE/CVF conference on computer vision and pattern recognition*, pages 8317–8326, 2019. 6
- [45] Dingjie Song, Wenjun Wang, Shunian Chen, Xidong Wang, Michael Guan, and Benyou Wang. Less is more: A simple yet effective token reduction method for efficient multimodal llms. *arXiv preprint arXiv:2409.10994*, 2024. 2
- [46] Ashish Vaswani, Noam Shazeer, Niki Parmar, Jakob Uszkoreit, Llion Jones, Aidan N Gomez, Łukasz Kaiser, and Illia Polosukhin. Attention is all you need. *Advances in neural information processing systems*, 30, 2017. 3
- [47] Peng Wang, Shuai Bai, Sinan Tan, Shijie Wang, Zhihao Fan, Jinze Bai, Keqin Chen, Xuejing Liu, Jialin Wang, Wenbin Ge, et al. Qwen2-vl: Enhancing vision-language model’s perception of the world at any resolution. *arXiv preprint arXiv:2409.12191*, 2024. 1
- [48] Weihang Wang, Qingsong Lv, Wenmeng Yu, Wenyi Hong, Ji Qi, Yan Wang, Junhui Ji, Zhuoyi Yang, Lei Zhao, Song XiXuan, et al. Cogvlm: Visual expert for pretrained language models. *Advances in Neural Information Processing Systems*, 37:121475–121499, 2025. 2
- [49] Dawei Yan, Pengcheng Li, Yang Li, Hao Chen, Qingguo Chen, Weihua Luo, Wei Dong, Qingsen Yan, Haokui Zhang, and Chunhua Shen. Tg-llava: Text guided llava via learnable latent embeddings. *arXiv preprint arXiv:2409.09564*, 2024. 3
- [50] Weihao Yu, Zhengyuan Yang, Linjie Li, Jianfeng Wang, Kevin Lin, Zicheng Liu, Xinchao Wang, and Lijuan Wang. Mm-vet: Evaluating large multimodal models for integrated capabilities. *arXiv preprint arXiv:2308.02490*, 2023. 6
- [51] Xiang Yue, Yuansheng Ni, Kai Zhang, Tianyu Zheng, Ruoqi Liu, Ge Zhang, Samuel Stevens, Dongfu Jiang, Weiming Ren, Yuxuan Sun, et al. Mmmu: A massive multi-discipline multimodal understanding and reasoning benchmark for expert agi. In *Proceedings of the IEEE/CVF Conference on Computer Vision and Pattern Recognition*, pages 9556–9567, 2024. 6
- [52] Qizhe Zhang, Aosong Cheng, Ming Lu, Zhiyong Zhuo, Minqi Wang, Jiajun Cao, Shaobo Guo, Qi She, and Shanghang Zhang. [cls] attention is all you need for training-free visual token pruning: Make vlm inference faster. *arXiv preprint arXiv:2412.01818*, 2024. 2
- [53] Shaolei Zhang, Qingkai Fang, Zhe Yang, and Yang Feng. Llava-mini: Efficient image and video large multimodal models with one visual token. *arXiv preprint arXiv:2501.03895*, 2025. 2
- [54] Yuan Zhang, Chun-Kai Fan, Junpeng Ma, Wenzhao Zheng, Tao Huang, Kuan Cheng, Denis Gudovskiy, Tomoyuki Okuno, Yohei Nakata, Kurt Keutzer, et al. Sparsevlm: Visual token sparsification for efficient vision-language model inference. *arXiv preprint arXiv:2410.04417*, 2024. 2
- [55] Yi-Fan Zhang, Qingsong Wen, Chaoyou Fu, Xue Wang, Zhang Zhang, Liang Wang, and Rong Jin. Beyond llava-hd: Diving into high resolution large multimodal models. *arXiv preprint arXiv:2406.08487*, 2024. 3
- [56] Deyao Zhu, Jun Chen, Xiaoqian Shen, Xiang Li, and Mohamed Elhoseiny. Minigpt-4: Enhancing vision-language understanding with advanced large language models. *arXiv preprint arXiv:2304.10592*, 2023. 2
- [57] Yuke Zhu, Chi Xie, Shuang Liang, Bo Zheng, and Sheng Guo. Focusllava: A coarse-to-fine approach for efficient and effective visual token compression. *arXiv preprint arXiv:2411.14228*, 2024. 3

## A. Visual results

### Count & Math



Q: How many giraffes are there in the image?

LLaVA-1.5: There is only **one** giraffe in the image.

InternVL2: There is **one** giraffe in the image.

InternVL-X: There are two giraffe in the image.

LLaVA-NeXT:  $7x + 5 - 3 = 10$  To solve for  $x$ , we can isolate  $x$  on one side of the equation:  $7x - 3 = 10$   $7x = 13$   $x = 13/7$  So the result of the bottom right equation is approximately 13/7

Q: What is the result of the bottom right equation, please answer a number.

InternVL2-HD: The answer of the bottom right equation,  $6 \times 5 = 30$ .

InternVL-X-HD:  $7 \times 5 - 3 = 32$ .

### Document

#### Scope and sequence

Module	Theme	Function	Structure
1 Wonders of the world (P2)	Nature and travel	Describing places and experiences	Comparison of present simple, past simple, future simple, present perfect, present continuous, past continuous
2 Public holidays (P10)	Festivals, holidays and celebrations	Talking about holiday plans	Adverbial clauses with <i>after, as soon as, before, since, until, where, while</i>
3 Heroes (P18)	Famous people	Giving reasons	Adverbial clauses with <i>because, so, so that</i>
4 Home alone (P26)	Life at home	Describing personal experiences	Adverbial clauses with <i>although, so...that</i>
5 Museums (P34)	Public rules and map reading	Talking about rules	Imperative sentences; adverbial clauses (4): <i>if...do</i>
6 Problems (P42)	Interpersonal communication	Describing problems and giving advice	Adverbial clauses (5): <i>if...will</i>
Revision module A (P50)			

Q: What is the theme corresponding to module "Museums" ?

LLaVA-NeXT: The theme corresponding to the module "Museums" is "Public rules and **talking about map reading**".

InternVL2-HD: The theme corresponding to the module "Museums" is " Public rules and **talking about map reading rules**".

InternVL-X-HD: The theme corresponding to the module "Museums" is "Public rules and map reading".

### Caption

Item	1994	1995	1996	1997	1998
Food	65%	60%	48%	42%	35%
Clothing	8%	9%	12%	15%	17%
Recreation	3%	5%	7%	8%	10%
Others	24%	26%	33%	35%	38%
Total	100%	100%	100%	100%	100%

Q: Please describe the image in detail, including specific numbers and the analysis

LLaVA-NeXT: The image is a table with a title "Table" at the bottom. The table is divided into six columns, each representing a different category: Item, Food, Clothing, Recreation, Others, and Total. Each category has a row of numbers corresponding to the years 1994, 1995, 1996, 1997, 1998, and 1999. In the **Item** column, the numbers range from 65% to 17%. In the Food column, the numbers range from 60% to 42%. In the Clothing column, the numbers range from 8% to 15%. In the Recreation column, the numbers range from 3% to 8%. In the Others column, the numbers range from 24% to 35%. In the Total column, the numbers range from 100% to 100%.

The table is presented in a simple, black and white format with no additional graphics or decorations. The numbers are organized in a structured manner, with each year's percentage values aligned to the left of the corresponding category. The table does not provide any additional context or explanation for the data.

InternVL2-HD: The image presents a table that provides a breakdown of various items and their corresponding percentages for the years 1994 to 1998. The table is organized into three columns: the item, the **percentage for 1994**, and the **percentage for 1995**. Starting from the top, the first item is "Food", which has a percentage of 65% in 1994 and 60% in 1995. The second item is "Clothing", with a percentage of 8% in 1994 and 9% in 1995. The third item is "Recreation", with a percentage of 3% in 1994 and 5% in 1995. The fourth item is "Others", with a percentage of 24% in 1994 and 26% in 1995. The table also includes a "Total" column, which shows the cumulative percentage for each year. For instance, the total percentage for 1994 is 100%, and for 1995, it is 100%.

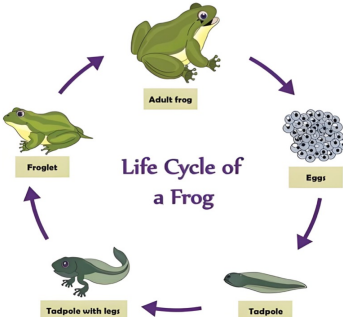
The table is neatly organized and provides a clear comparison of the percentages of these items over the two years. The percentages are presented in a simple and straightforward manner, making it easy to understand the changes in each item's percentage over time.

InternVL-X-HD: The image presents a table that provides a breakdown of various items and their respective percentages for the years 1994 to 1998. The table is organized into three columns: the year, the item, and the percentage.

Starting from the top, the first item listed is "Food", which is 65% in 1994, decreasing to 35% in 1998. The second item is "Clothing", which was 8% in 1994, increasing to 17% in 1998. The third item is "Recreation", which was 3% in 1994, increasing to 10% in 1998. The fourth item is "Others", which was 24% in 1994, decreasing to 38% in 1998. The table also includes a "Total" column, which shows that the total percentage for all items remained constant at 100% for each year. This suggests that the percentages for each item were adjusted to maintain the overall total.

The table is a useful tool for understanding trends in consumer spending over time. It shows that the percentage of spending on clothing and recreation increased, while the percentage of spending on food and **others decreased**. This could be due to various factors such as changes in consumer preferences, economic conditions, or shifts in the market.

### Visual reasoning



Q: How many steps from an egg to a froglet? answer it with a number.

LLaVA-1.5: **10**.

InternVL2: **Four steps**.

InternVL-X: **3**.

### Visual perception



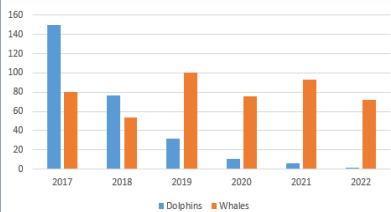
Q: What color are the scissors in the image?

LLaVA-1.5: The scissors in the image are **red**.

InternVL2: The scissors are **red and green**.

InternVL-X: The scissors in the image are green.

### Chart



Q: Which year does the "dolphins" metric have the second highest value? answer it with a year

LLaVA-1.5: **2019**.

InternVL2: **2022**.

InternVL-X: **2018**.

### Visual perception



Q: What is the vehicle number of the bus?

LLaVA-1.5: The vehicle number of the bus is **393**.

InternVL2: The vehicle number of the bus is **55a**.

InternVL-X: The vehicle number of the bus is 588.

Figure 9. Visual comparison of InternVL-X with other models. Red fonts represent incorrect answers.